HHS Public Access

Author manuscript

J Am Chem Soc. Author manuscript; available in PMC 2021 May 20.

Published in final edited form as:

J Am Chem Soc. 2020 May 20; 142(20): 9158–9162. doi:10.1021/jacs.0c03672.

Molecular-level control over plasmonic properties in silver nanoparticle/self-assembling peptide hybrids

Yin Wang[1,2], **Xiaozhou Yang**[1], **Tianyu Liu**[1], **Zhao Li**[1,2], **David Leskauskas**[1], **Guoliang Liu**[*,1,2], **John B. Matson**[*,1,2]

[1]Department of Chemistry, Virginia Tech, Blacksburg, VA 24061, United States

[2]Macromolecules Innovation Institute, Virginia Tech, Blacksburg, VA 24061, United States

Abstract

The plasmonic properties of AgNP arrays are directly controlled by AgNP size, shape, and spatial arrangement. Reported here is a strategy to prepare chiral AgNP arrays templated by two constitutionally isomeric aromatic peptide amphiphiles (APAs), $\mathbf{K_S}\boldsymbol{C'}\mathbf{EK_S}$ and $\boldsymbol{C'}\mathbf{EK_SK_S}$ (K_S= *S*-aroylthiooxime-modified lysine, *C'*= citrulline, and E=glutamic acid). In phosphate buffer, both APAs initially self-assembled into nanoribbons with a similar geometry. However, in the presence of silver ions and poly(sodium 4-styrenesulfonate) (PSSS), one of nanoribbons ($\mathbf{K_S}\boldsymbol{C'}\mathbf{EK_S}$) turned into nanohelices with a regular twisting pitch, while the other ($\boldsymbol{C'}\mathbf{EK_SK_S}$) remained as nanoribbons. Both were used as templates for synthesis of arrays of ~8 nm AgNPs to understand how small changes in molecular structure affect the plasmonic properties of these chiral AgNP/APA hybrids. Both hybrids showed improved colloidal stability compared to pure AgNPs, and both showed enhanced sensitivity as surface-enhanced Raman spectroscopy (SERS) substrates for model analytes, with nanohelices showing better SERS performance compared to their nanoribbon-counterparts and pure AgNPs.

Silver nanoparticles (AgNPs) are suitable substrates for catalysis,[1–2] sensing,[3–4] and antimicrobial applications,[5–6] and their properties depend heavily on their size, shape, and spatial arrangement.[7–8] Therefore, synthesis of AgNPs with well-defined dimensions and controlled spatial arrangements allows researchers to tune the properties of these materials for specific functions. Toward this end, materials including carbon nanotubes,[2] polymers,[9–11] DNA,[12–13] and peptides[14–15] have been used as scaffolds to direct the growth or assembly of AgNPs, relying on strong interactions between AgNPs or their precursors and functional groups on these scaffolds. Among these, self-assembled peptides are particularly attractive platforms for AgNP growth[16–19] because of their chemical tunability and their capacity to self-assemble into a wide variety of morphologies, including nanoribbons, nanosheets, and nanohelices, among others.[20–24] For instance, nanofibers assembled from aldehyde-functionalized peptide amphiphiles were used to template the growth of AgNPs in the presence of Tollens' solution.[16] Particularly intriguing are self-assembled peptide-based

*Corresponding Authors: gliu1@vt.edu, jbmatson@vt.edu.

Supporting Information. The Supporting Information is available free of charge on the ACS Publications website. Detailed experimental section and additional characterization (ESI-MS, UV–Vis, circular dichroism)

The authors declare no competing financial interest.

helical nanoribbons,[17] which organize achiral AgNPs into chiral assemblies. However, the structure-property relationships among the molecular composition of the template, the spatial arrangements of the AgNPs, and the resultant plasmonic properties of the hybrids remain elusive.

We recently discovered a class of constitutionally isomeric aromatic peptide amphiphiles (APAs) that self-assemble into different morphologies depending on the specific peptide sequence.[25] The key component of these APAs, each made of four amino acids, is the inclusion of two lysine residues that contain aromatic *S*-aroylthiooxime (SATO) functional groups[26] attached to their ε-amines.[27–31] We viewed these APAs as templates for AgNP growth, which would enable the AgNP/APA hybrids to retain the chiral imprint from the APA nanostructures. Because these APAs are constitutional isomers, we envisioned that we could control the spatial arrangements of AgNPs and therefore, the plasmonic properties of the hybrids by simply changing the order of amino acids. In this context, we report here that silver salts induce a morphological transition in two constitutionally isomeric APAs, which we used as the templates for AgNP growth. Our results showed that the APA morphology affected the spatial arrangements of AgNPs, which influenced the plasmonic properties of the hybrids, and as a result, their sensitivity as substrates for surface-enhanced Raman spectroscopy (SERS).

We synthesized two constitutionally isomeric APAs that each contained one glutamic acid (E), one citrulline (*C'*), and two SATO-modified lysine (K_S) residues: $\mathbf{K_S}\boldsymbol{C'}\mathbf{EK_S}$ and $\boldsymbol{C'}\mathbf{EK_SK_S}$ (Figures 1A–B, S1–2). Based on our previous studies on APAs with similar structures,[25] we expected that $\mathbf{K_S}\boldsymbol{C'}\mathbf{EK_S}$ and $\boldsymbol{C'}\mathbf{EK_SK_S}$ would form different self-assembled morphologies due to the different arrangements of amino acids in their structures. However, we were surprised to find that both APAs assembled into one-dimensional nanostructures with similar morphologies based on transmission electron microscopy (TEM) observations (Figures 1C and 1D). $\mathbf{K_S}\boldsymbol{C'}\mathbf{EK_S}$ formed nanoribbons with average widths of 7 ± 1 nm and lengths of a few micrometers (Figure 1C). $\boldsymbol{C'}\mathbf{EK_SK_S}$ also assembled into micrometer-long nanoribbons with average widths of 6 ± 1 nm, (Figure 1D). Next, we added silver nitrate ($AgNO_3$, 0.5 mM) and poly(sodium 4-styrenesulfonate) (PSSS, 0.5 mg mL^{-1}) to induce AgNP formation, which we typically use in AgNP synthesis.[32] Interestingly, upon addition of $AgNO_3$ and PSSS, the $\mathbf{K_S}\boldsymbol{C'}\mathbf{EK_S}$ nanoribbons changed into micrometer-long nanohelices with an average diameter of 6 ± 1 nm and a regular twisting pitch of 29 ± 5 nm (Figure 1E). In sharp contrast, APA $\boldsymbol{C'}\mathbf{EK_SK_S}$ retained its nanoribbon morphology after adding $AgNO_3$ and PSSS, although the average length decreased (Figure 1F). The distinct morphology differences between $\mathbf{K_S}\boldsymbol{C'}\mathbf{EK_S}$ and $\boldsymbol{C'}\mathbf{EK_SK_S}$ before and after salt addition exemplify how small changes in APA sequence can lead to dramatically different self-assembly behaviors.

Next, molecular packing within self-assembled APAs before and after addition of $AgNO_3$ and PSSS was assessed by circular dichroism (CD) spectroscopy. Before adding salts, both $\mathbf{K_S}\boldsymbol{C'}\mathbf{EK_S}$ and $\boldsymbol{C'}\mathbf{EK_SK_S}$ displayed a classical β-sheet secondary structure, along with a strong SATO absorption (Figure S3). Interestingly, the CD spectra were nearly identical mirror images; this inversion likely resulted from different handedness of the assemblies.[27, 33] When $AgNO_3$ and PSSS were added to the solution, the spectrum changed into a random coil-like structure for $\mathbf{K_S}\boldsymbol{C'}\mathbf{EK_S}$ (the same as when only PSSS was added to the

solution). However, the spectrum did not change significantly for ***C'*EK$_S$K$_S$**. These changes were consistent with TEM observations, where **K$_S$*C'*EK$_S$** showed significant morphological changes after salt addition, but ***C'*EK$_S$K$_S$** did not.

We next used these two nanostructured templates to synthesize AgNP/APA hybrids in a two-step process (Figure S4A). In the first step, we added $AgNO_3$ and PSSS to a **K$_S$*C'*EK$_S$** solution, followed by the reducing agent $NaBH_4$. The solution changed from colorless to yellow, suggesting the formation of small Ag seeds (AgSDs).[32] A UV-Vis spectrum showed a peak near 405 nm (Figure S4B), consistent with the characteristic plasmonic response for non-aggregated, spherical AgNPs smaller than 10 nm.[34] In the second step, additional $AgNO_3$ solution was added dropwise into an aliquot of AgSDs (50–1000 μL) and ascorbic acid. During this second growth step, the color of the solution became bright yellow, with the peak absorption remaining at 405 nm (Figure S4B). We determined that both a minimum amount of AgSDs and PSSS were required for maintaining the **K$_S$*C'*EK$_S$** nanohelix morphology in the resultant AgNP/**K$_S$*C'*EK$_S$** hybrids. Addition of too little AgSD solution resulted in the formation of nanoribbons (Figure S5), as did excluding PSSS from the synthesis (Figure S7). We then used this optimized procedure to prepare AgSDs and AgNPs templated by the ***C'*EK$_S$K$_S$** nanoribbons, which showed the same color change in each step as the AgSDs and AgNPs templated by the **K$_S$*C'*EK$_S$** nanohelices.

TEM was then used to examine the morphologies of the AgNP/APA hybrids and measure the sizes of the AgSDs and AgNPs in both samples. The growth of AgSDs and AgNPs had little influence on the original morphologies of these two different self-assembled APAs (Figures 2A–D). In the presence of **K$_S$*C'*EK$_S$** nanohelices, the diameter of the AgSDs was 2.8 ± 0.5 nm (Figure 2A). After the second round of Ag growth, the diameter of the AgNPs increased to 7.6 ± 0.9 nm (Figure 2C). When ***C'*EK$_S$K$_S$** nanoribbons were used as the template under the same growth conditions, AgSDs and AgNPs formed with diameters of 2.9 ± 0.6 nm (Figure 2B) and 8 ± 1 nm (Figure 2D), respectively. Although the sizes of the AgSDs and the AgNPs were similar on both the nanohelices and the nanoribbons, the AgSDs and AgNPs were distributed mostly within the **K$_S$*C'*EK$_S$** nanohelices (Figures 2A and 2C), while those templated by the ***C'*EK$_S$K$_S$** nanoribbons distributed at the edges of the nanoribbons (Figures 2B and 2D). We also prepared AgNP/**K$_S$*C'*EK$_S$** hybrids without PSSS, which as we noted above was vital for nanohelix formation (Figure S7). These AgSD and AgNP arrays had similar appearance and dimensions (2.6 ± 0.9 nm for AgSDs and 8 ± 1 nm for AgNPs) to the nanoribbon-forming AgNP/***C'*EK$_S$K$_S$** hybrids. These results demonstrate that both APAs functioned as templates for AgNP growth, regulating the spatial arrangement of these nanoparticles.

CD spectroscopy allowed us to investigate the chirality of the resultant hybrids. The CD spectrum of AgNP/**K$_S$*C'*EK$_S$** displayed three negative peaks at 386, 407, and 471 nm (Figure 2E), whereas that of AgNP/***C'*EK$_S$K$_S$** exhibited only a broad negative peak with a minimum at 414 nm (Figure 2F). For an achiral assembly of AgNPs, a flat CD spectrum would be expected, so these spectra confirm that chirality was transferred from the APA nanoassemblies to these hybrid structures, similar to AgNPs templated by DNA.[13] In addition, the absorption beyond 470 nm was much stronger for AgNP/**K$_S$*C'*EK$_S$** than for

AgNP/***C'*EK$_S$K$_S$**; this spectral feature may indicate a stronger interaction between AgNPs and **K$_S$*C'*EK$_S$** nanohelices than ***C'*EK$_S$K$_S$** nanoribbons.[35]

Next, we evaluated the stability of the AgNP/APA hybrids through multiple lyophilization cycles, as this property is critical for storage, transportation, and further practical applications. The stability was assessed by measuring the intensity of the localized surface plasmonic resonance (LSPR) absorption of the AgNPs at 405 nm, which reflects the concentration of dispersed AgNPs in solution. The absorbance of all hybrids and pure AgNPs of similar size decreased with each lyophilization cycle (Figures 3A and S8). Specifically, the absorbance of the helical AgNP/**K$_S$*C'*EK$_S$** hybrids decreased to 80% of its original value after one lyophilization cycle, while nanoribbon-forming AgNP/***C'*EK$_S$K$_S$** hybrids decreased to 55%. Similarly, the absorption of AgNP/**K$_S$*C'*EK$_S$** nanoribbons prepared without PSSS decreased to 58% after one lyophilization cycle. The absorption of pure AgNPs (without any APA template) after one cycle decreased to 5% of its original value. Notably, all the hybrids could be re-hydrated and re-suspended after several cycles of lyophilization, while pure AgNPs could not. We conducted similar colloidal stability studies by adding increasing amounts of salt (PB) to these three types of AgNP/APA hybrids along with pure AgNPs (Figure S9). Results showed that all AgNP/APA hybrids tolerated salt better than pure AgNPs.

Finally, given the different spatial arrangements of AgNPs on the self-assembled APAs, we asked whether these hybrids could be used as substrates for SERS. Specifically, we investigated whether APA morphology in these AgNP/APA hybrids would affect SERS sensitivity. We selected rhodamine B (RhB) and 2,2'-bipyridine (Bpy) as model SERS analytes. Notably, for both analytes, the helical AgNP/**K$_S$*C'*EK$_S$** hybrids outperformed all other materials investigated. In the case of RhB, it enhanced the characteristic Raman bands to a much greater extent than the two nanoribbon-forming controls, AgNP/***C'*EK$_S$K$_S$** and AgNP/**K$_S$*C'*EK$_S$** without PSSS (Figure 3B). Additional control systems including pure AgNPs (no APA template) as well as the APAs **K$_S$*C'*EK$_S$** and ***C'*EK$_S$K$_S$** without AgNPs were also investigated for comparison. The pure AgNPs displayed a weak SERS signal, while the APAs alone showed no discernable SERS signal. We also observed the same trend of SERS enhancement when Bpy was used as the analyte (Figure S10).

These results indicate that the spatial arrangement of AgNPs into the helical configuration provided by **K$_S$*C'*EK$_S$** is key for superior SERS enhancement over its nanoribbon-forming counterparts because the size and shape of the AgNPs investigated were the same. We hypothesize that AgNPs within the grooves of **K$_S$*C'*EK$_S$** nanohelices were better immobilized and provided a more favorable 3D arrangement for SERS than the AgNPs on the nanoribbons (***C'*EK$_S$K$_S$** or **K$_S$*C'*EK$_S$** without PSSS). Compared to commonly used SERS substrates that are either plasmonic NPs grafted with ligands or lithographically patterned metal surfaces,[36–39] our constructs provide unique particle arrangements, require negligible energy input, possess high colloidal stability, and are dispersible in biological media.

In summary, we have reported a simple strategy to construct chiral AgNP hybrids from two APAs, **K$_S$*C'*EK$_S$** and ***C'*EK$_S$K$_S$**, both of which initially assembled into nanoribbons with

similar dimensions. However, when silver ions and PSSS were added, one of nanoribbons (**K_S*C'*EK$_S$**) transformed into nanohelices. Both nanostructures served as effective templates for AgNP growth, and the resulting hybrids showed improved stability over pure AgNPs. We found that these hybrid materials were suitable as SERS substrates, with the nanohelix-forming hybrids exhibiting a superior signal enhancement driven by the unique spatial arrangement of AgNPs compared to their nanoribbon counterparts. This work highlights how small changes in molecular structure can dramatically alter plasmonic properties. We believe this strategy reveals novel ways to construct sophisticated peptide-based nanostructures for biomedical applications such as biomarker detection.

Supplementary Material

Refer to Web version on PubMed Central for supplementary material.

Acknowledgments

This work was supported by the Virginia Tech Dean's Discovery Fund, the National Science Foundation (DMR-1454754 and DMR-1752611), and the National Institutes of Health (R01GM123508). We thank Prof Tijana Grove (Virginia Tech) and her students for experimental assistance, Prof Peter Vikesland for helpful discussions, and Samantha J. Scannelli and Kearsley M. Dillon for careful readings of the manuscript. The authors acknowledge use of facilities within the Nanoscale Characterization and Fabrication Laboratory at Virginia Tech.

References

1. Kundu S Formation of self-assembled Ag nanoparticles on DNA chains with enhanced catalytic activity. Phys. Chem. Chem. Phys 2013, 15, 14107–14119. [PubMed: 23872921]
2. Singh P; Lamanna G; Menard-Moyon C; Toma FM; Magnano E; Bondino F; Prato M; Verma S; Bianco A Formation of efficient catalytic silver nanoparticles on carbon nanotubes by adenine functionalization. Angew. Chem. Int. Ed 2011, 50, 9893–9897.
3. Yao J; Yang M; Duan YX Chemistry, biology, and medicine of fluorescent nanomaterials and related systems: new insights into biosensing, bioimaging, genomics, diagnostics, and therapy. Chem. Rev 2014, 114, 6130–6178. [PubMed: 24779710]
4. Zeng SW; Baillargeat D; Ho HP; Yong KT Nanomaterials enhanced surface plasmon resonance for biological and chemical sensing applications. Chem. Soc. Rev 2014, 43, 3426–3452. [PubMed: 24549396]
5. Rizzello L; Pompa PP Nanosilver-based antibacterial drugs and devices: Mechanisms, methodological drawbacks, and guidelines. Chem. Soc. Rev 2014, 43, 1501–1518. [PubMed: 24292075]
6. Rai M; Yadav A; Gade A Silver nanoparticles as a new generation of antimicrobials. Biotechnol. Adv 2009, 27, 76–83. [PubMed: 18854209]
7. Wiley B; Sun YG; Xia YN Synthesis of silver nanostructures with controlled shapes and properties. Acc. Chem. Res 2007, 40, 1067–1076. [PubMed: 17616165]
8. Nie ZH; Petukhova A; Kumacheva E Properties and emerging applications of self-assembled structures made from inorganic nanoparticles. Nat. Nanotechnol 2010, 5, 15–25. [PubMed: 20032986]
9. Huang F; Gao Y; Zhang YM; Cheng TJ; Ou HL; Yang LJ; Liu JJ; Shi LQ; Liu JF Silver-decorated polymeric micelles combined with curcumin for enhanced antibacterial activity. ACS Appl. Mater. Interfaces 2017, 9, 16881–16890.
10. Hoque J; Yadav V; Prakash RG; Sanyal K; Haldar J Dual-function polymer-silver nanocomposites for rapid killing of microbes and inhibiting biofilms. ACS Biomater. Sci. Eng 2019, 5, 81–91.

11. Li RC; Wang H; Song Y; Lin YN; Dong M; Shen YD; Khan S; Zhang SY; Fan JW; Zhang FW; Su L; Wooley KL *In situ* production of Ag/polymer asymmetric nanoparticles via a powerful light-driven technique. J. Am. Chem. Soc 2019, 141, 19542–19545. [PubMed: 31820965]
12. Pal S; Sharma J; Yan H; Liu Y Stable silver nanoparticle-DNA conjugates for directed self-assembly of core-satellite silver-gold nanoclusters. Chem. Comm 2009, 6059–6061. [PubMed: 19809643]
13. Shemer G; Krichevski O; Markovich G; Molotsky T; Lubitz I; Kotlyar AB Chirality of silver nanoparticles synthesized on DNA. J. Am. Chem. Soc 2006, 128, 11006–11007. [PubMed: 16925401]
14. Vasylevskyi SI; Kracht S; Corcosa P; Fromm KM; Giese B; Fueg M Formation of silver nanoparticles by electron transfer in peptides and c-cytochromes. Angew. Chem. Int. Ed 2017, 56, 5926–5930.
15. Kalakonda P; Banne S Synthesis and optical properties of highly stabilized peptide-coated silver nanoparticles. Plasmonics 2018, 13, 1265–1269.
16. Pazos E; Sleep E; Perez CMR; Lee SS; Tantakitti F; Stupp SI Nucleation and growth of ordered arrays of silver nanoparticles on peptide nanofibers: hybrid nanostructures with antimicrobial properties. J. Am. Chem. Soc 2016, 138, 5507–5510. [PubMed: 27103596]
17. Lin YY; Pashuck ET; Thomas MR; Amdursky N; Wang ST; Chow LW; Stevens MM Plasmonic chirality imprinting on nucleobase-displaying supramolecular nanohelices by metal-nucleobase recognition. Angew. Chem. Int. Ed 2017, 56, 2361–2365.
18. Diez I; Hahn H; Ikkala O; Borner HG; Ras RHA Controlled growth of silver nanoparticle arrays guided by a self-assembled polymer-peptide conjugate. Soft Matter 2010, 6, 3160–3162.
19. Reithofer MR; Lakshmanan A; Ping ATK; Chin JM; Hauser CAE *In situ* synthesis of size-controlled, stable silver nanoparticles within ultrashort peptide hydrogels and their anti-bacterial properties. Biomaterials 2014, 35, 7535–7542. [PubMed: 24933510]
20. Matson JB; Stupp SI Self-assembling peptide scaffolds for regenerative medicine. Chem. Comm 2012, 48, 26–33. [PubMed: 22080255]
21. Wang Y; Cheetham AG; Angacian G; Su H; Xie LS; Cui HG Peptide-drug conjugates as effective prodrug strategies for targeted delivery. Adv. Drug Delivery Rev 2017, 110, 112–126.
22. Fleming S; Ulijn RV Design of nanostructures based on aromatic peptide amphiphiles. Chem. Soc. Rev 2014, 43, 8150–8177. [PubMed: 25199102]
23. Worthington P; Langhans S; Pochan D beta-hairpin peptide hydrogels for package delivery. Adv. Drug Deliv. Rev 2017, 110, 127–136. [PubMed: 28257999]
24. Hamley IW Small bioactive peptides for biomaterials design and therapeutics. Chem. Rev 2017, 117, 14015–14041. [PubMed: 29227635]
25. Wang Y; Kaur K; Scannelli SJ; Bitton R; Matson JB Self-assembled nanostructures regulate H_2S release from constitutionally isomeric peptides. J. Am. Chem. Soc 2018, 140, 14945–14951. [PubMed: 30369241]
26. Foster JC; Powell CR; Radzinski SC; Matson JB *S*-aroylthiooximes: A facile route to hydrogen sulfide releasing compounds with structure-dependent release kinetics. Org. Lett 2014, 16, 1558–1561. [PubMed: 24575729]
27. Wang Y; Matson JB Supramolecular nanostructures with tunable donor loading for controlled H_2S release. ACS Appl. Bio Mater 2019, 2, 5093–5098.
28. Qian Y; Kaur K; Foster JC; Matson JB Supramolecular tuning of H_2S release from aromatic peptide amphiphile gels: Effect of core unit substituents. Biomacromolecules 2019, 20, 1077–1086. [PubMed: 30676716]
29. Kaur K; Wang Y; Matson JB Linker-regulated H_2S release from aromatic peptide amphiphile hydrogels. Biomacromolecules 2020, 21, 1171–1178. [PubMed: 32053359]
30. Longchamp A; Kaur K; Macabrey D; Dubuis C; Corpataux JM; Deglise S; Matson JB; Allagnat F Hydrogen sulfide-releasing peptide hydrogel limits the development of intimal hyperplasia in human vein segments. Acta Biomater. 2019, 97, 374–384. [PubMed: 31352106]
31. Carter JM; Qian Y; Foster JC; Matson JB Peptide-based hydrogen sulphide-releasing gels. Chem. Commun 2015, 51, 13131–13134.

32. Khan AU; Zhou ZP; Krause J; Liu GL Poly(vinylpyrrolidone)-free multistep synthesis of silver nanoplates with plasmon resonance in the near infrared range. Small 2017, 13, 1701715.

33. Xing QG; Zhang JX; Xie YY; Wang YF; Qi W; Rao HJ; Su RX; He ZM Aromatic motifs dictate nanohelix handedness of tripeptides. ACS Nano 2018, 12, 12305–12314. [PubMed: 30452865]

34. Khan AU; Zhao SQ; Liu GL Key parameter controlling the sensitivity of plasmonic metal nanoparticles: Aspect ratio. J. Phys. Chem. C 2016, 120, 19353–19364.

35. Maoz BM; van der Weegen R; Fan ZY; Govorov AO; Ellestad G; Berova N; Meijer EW; Markovich G Plasmonic chiroptical response of silver nanoparticles interacting with chiral supramolecular assemblies. J. Am. Chem. Soc 2012, 134, 17807–17813. [PubMed: 23039182]

36. Wang H; Levin CS; Halas NJ Nanosphere arrays with controlled sub-10-nm gaps as surface-enhanced Raman spectroscopy substrates. J. Am. Chem. Soc 2005, 127, 14992–14993. [PubMed: 16248615]

37. Guerrini L; Graham D Molecularly-mediated assemblies of plasmonic nanoparticles for surface-enhanced raman spectroscopy applications. Chem. Soc. Rev 2012, 41, 7085–7107. [PubMed: 22833008]

38. Sharma B; Frontiera RR; Henry AI; Ringe E; Van Duyne RP SERS: Materials, applications, and the future. Mater. Today 2012, 15, 16–25.

39. Tessier P; Velev OD; Kalambur AT; Lenhoff AM; Rabolt JF; Kaler EW Structured metallic films for optical and spectroscopic applications via colloidal crystal templating. Adv. Mater 2001, 13, 396–400.

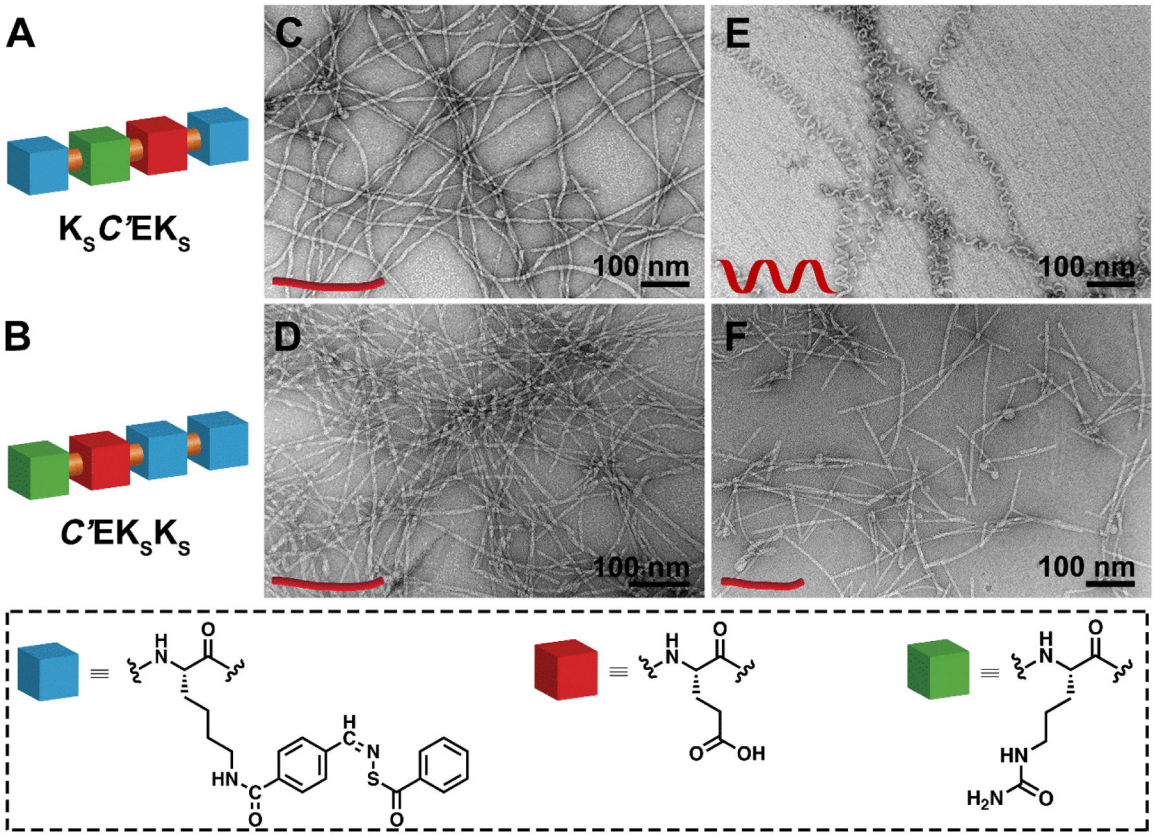

Figure 1.

(A and B) Schematic illustrations of the chemical structures of the two isomeric APAs. (C–F) TEM images of (C) nanoribbons formed by $\mathbf{K_S C'EK_S}$ and (D) $\mathbf{C'EK_SK_S}$ in 10 mM PB; (E) nanohelices derived from $\mathbf{K_S C'EK_S}$ and (F) short nanoribbons assembled by $\mathbf{C'EK_SK_S}$ in 10 mM PB containing $AgNO_3$ and PSSS.

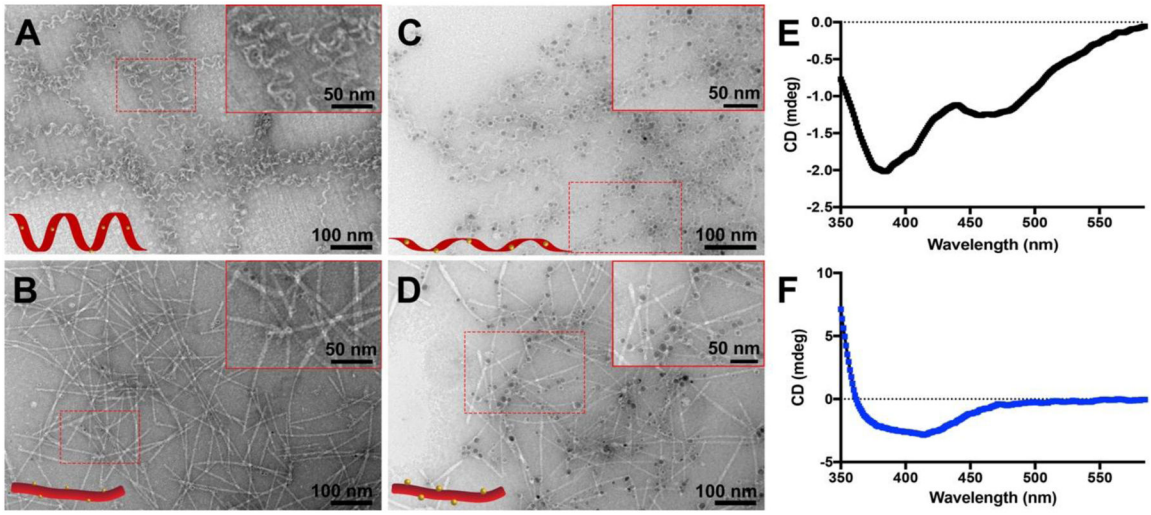

Figure 2.

(A-D) TEM images of (A) AgSD/$\mathbf{K_S}\boldsymbol{C'}\mathbf{EK_S}$ nanohelices, (B) AgSD/$\boldsymbol{C'}\mathbf{EK_S}\mathbf{K_S}$ nanoribbons, (C) AgNP/$\mathbf{K_S}\boldsymbol{C'}\mathbf{EK_S}$ nanohelices, and (D) AgNP/$\boldsymbol{C'}\mathbf{EK_S}\mathbf{K_S}$ nanoribbons. Inserts in the top right corners of panels A–D show zoomed-in images of the areas outlined by the dashed red rectangles. (E and F) CD spectra of (E) AgNP/$\mathbf{K_S}\boldsymbol{C'}\mathbf{EK_S}$ nanohelices and (F) AgNP/$\boldsymbol{C'}\mathbf{EK_S}\mathbf{K_S}$ nanoribbons.

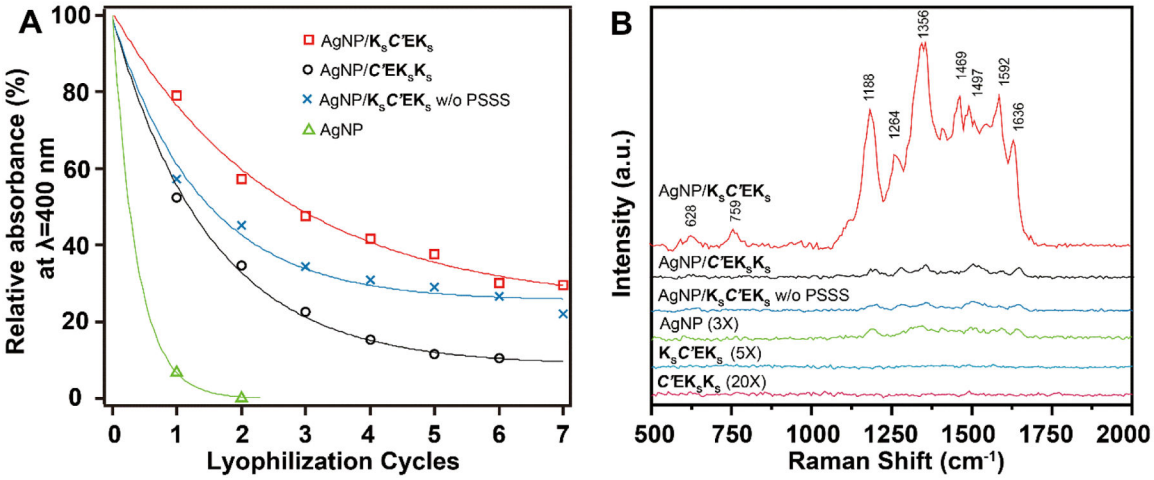

Figure 3.

(A) Colloidal stability of all groups studied in the present work against lyophilization. Comparing the decay rates of the intensities of the LSPR absorbance peak corresponding to AgNPs ($\lambda_{LSPR} \approx 405$ nm) indicates the resistance of AgNPs to aggregation. The peak intensity prior to lyophilization serves as a reference for normalization (100 % relative absorbance). Data were fitted with an exponential model (See Supporting Information for details). (B) SERS spectra of 10^{-4} M RhB collected on AgNP/APA hybrids with different morphologies, pure AgNPs, and pure APAs. Spectra of controlled samples were intensified as indicated for better visualization.